NUMERICAL MODELING OF BACKFILLING PROCESS AROUND MONOPILES

Cüneyt Baykal[1], B. Mutlu Sumer[2], David R. Fuhrman[2], Niels G. Jacobsen[3] and Jørgen Fredsøe[2]

This study presents a three-dimensional (3D) numerical modeling study on the backfilling process around monopiles. The numerical model utilized in the study is based on that given by Jacobsen (2011). It is composed of two main modules. The first module is the hydrodynamic model where the fluid flow conditions around the structure and near the bed are solved. The second module is the morphologic model where the sediment transport rates over the bed and around the structure are obtained and used in updating bed elevations around the structure. In the numerical model, the hydrodynamic computations are followed by morphologic computations, resulting in updated bed elevations and mesh structure which are again used to update the hydrodynamics for the next time step. In the hydrodynamic model, Reynolds-averaged Navier-Stokes (RANS) equations are solved with a k-ω turbulence closure. The morphologic model comprises five sub-modules, namely bed load, suspended load, sand slide, bed evolution and 3D mesh motion. The model is constructed in OpenFOAM CFD Package. The present model is applied to several problems of backfilling around a monopile by waves only, where the initial scour hole is generated by steady current. The numerical results appear to be in accord with the existing experimental information.

INTRODUCTION

The seabed around an offshore wind turbine foundation continuously experiences scour and backfilling in an alternating fashion under an ever changing wave and current climate. Engineering models have been developed with the purpose of predicting the time history of scour and backfilling for large times (weeks, months, or years), Nielsen and Hansen (2007), Raaijmakers and Rudolph (2008 a and b), and Harris et al. (2010). These models have essentially two components: scour and backfilling. The existing information on scour has been successfully incorporated in the models. This is not so, however, for the backfilling because of the lack of knowledge.

Previously, Fredsøe et al. (1992) studied backfilling in the case of a pipeline, and Hartvig et al. (2010) in the case of a pile, both with limited coverage. Recently, Sumer et al. (2013) have reported the results of an experimental study on backfilling around piles exposed to waves and currents. The latter has shed light onto the understanding of the backfilling process. It has also presented a comprehensive set of data on various properties of the backfilling process, particularly for the time scale, a crucially important quantity used in the development of engineering models such as those mentioned in the preceding paragraph. The present study continues the investigation of the backfilling numerically. The developed numerical model has been tested and validated against Sumer et (2013) al.'s experiments.

HYDRODYNAMIC MODEL

Governing equations

The numerical model solves the incompressible Reynolds-averaged Navier-Stokes equations

$$\frac{\partial u_i}{\partial t} + u_j \frac{\partial u_i}{\partial x_j} = -\frac{1}{\rho}\frac{\partial p}{\partial x_i} + \frac{\partial}{\partial x_j}\left[2\nu S_{ij} + \frac{\tau_{ij}}{\rho}\right] \tag{1}$$

combined with the continuity equation

$$\frac{\partial u_i}{\partial x_i} = 0 \tag{2}$$

Here, S_{ij} is the mean-strain-rate tensor

[1] Middle East Technical University, Dept. of Civil Eng., Ocean Eng. Res. Centre, Dumlupınar Blv. 06800 Çankaya, Ankara, Turkey (on leave from Dept. of Mechanical Eng., Section for Fluid Mechanics, Coastal and Maritime Eng., Technical University of Denmark, DK-2800 Kgs. Lyngby, Denmark)
[2] Dept. of Mechanical Eng., Section for Fluid Mechanics, Coastal and Maritime Eng., Technical University of Denmark, DK-2800 Kgs. Lyngby, Denmark
[3] Deltares, Department of Coastal Structures and Waves, Boussinesqweg 1, 2629HV Delft, The Netherlands (on leave from Dept. of Mechanical Eng., Section for Fluid Mechanics, Coastal and Maritime Eng., Technical University of Denmark, DK-2800 Kgs. Lyngby, Denmark)

$$S_{ij} = \frac{1}{2}\left(\frac{\partial u_i}{\partial x_j} + \frac{\partial u_j}{\partial x_i} \right),$$

(3)

u_i are the mean velocities (phase-resolved in the case of waves), x_i are the Cartesian coordinates, t is time, p is the pressure, v is the fluid kinematic viscosity, ρ is the fluid density, and τ_{ij} is the Reynolds stress tensor. The latter quantity is defined according to the following constitutive relation:

$$\frac{\tau_{ij}}{\rho} = -\overline{u_i' u_j'} = 2v_T S_{ij} - \frac{2}{3} k \delta_{ij}$$

(4)

in which δ_{ij} is the Kronecker delta, v_T is the eddy viscosity, and k is the turbulent kinetic energy density

$$k = \frac{1}{2}\overline{u_i' u_i'}$$

(5)

The turbulence closure is achieved by the two-equation k-ω turbulence model of Wilcox (2006, 2008). Based on the authors' experience, the present model can be expected to behave similarly to other k-ω variants, e.g. the k-ω SST models used in our previous studies of Roulund et al. (2005) and Dixen et al. (2013), while requiring fewer closure coefficients. Wilcox (2006) further discusses the new version of the k-ω, the version used in the present study, and earlier versions created by Wilcox et al., see Wilcox (2006, p. 127 and p. 152).

In the present model the eddy viscosity is defined by

$$v_T = \frac{k}{\tilde{\omega}}, \qquad \tilde{\omega} = \max\left\{ \omega, C_{\lim}\sqrt{\frac{2S_{ij}}{\beta^*}} \right\}$$

(6)

which incorporates a stress limiting feature, with $C_{lim}=7/8$. The model equations for the quantities k and ω read as follows

$$\frac{\partial k}{\partial t} + u_j \frac{\partial k}{\partial x_j} = \frac{\tau_{ij}}{\rho} \frac{\partial u_i}{\partial x_j} - \beta^* k \omega + \frac{\partial}{\partial x_j}\left[\left(v + \sigma^* \frac{k}{\omega} \right) \frac{\partial k}{\partial x_j} \right],$$

(7)

$$\frac{\partial \omega}{\partial t} + u_j \frac{\partial \omega}{\partial x_j} = \alpha \frac{\omega}{k} \frac{\tau_{ij}}{\rho} \frac{\partial u_i}{\partial x_j} - \beta \omega^2 + \frac{\sigma_d}{\omega} \frac{\partial k}{\partial x_j} \frac{\partial \omega}{\partial x_j} + \frac{\partial}{\partial x_j}\left[\left(v + \sigma \frac{k}{\omega} \right) \frac{\partial \omega}{\partial x_j} \right],$$

(8)

in which ω is the specific dissipation rate defined by

$$\omega = \frac{\varepsilon}{k \beta^*}$$

(9)

with ε being the dissipation of turbulent kinetic energy

$$\varepsilon = v \overline{\frac{\partial u_i'}{\partial x_k} \frac{\partial u_i'}{\partial x_k}}$$

(10)

The quantity σ_d in Eq. 8 is

$$\sigma_d = H\left\{ \frac{\partial k}{\partial x_j} \frac{\partial \omega}{\partial x_j} \right\} \sigma_{d0},$$

(11)

in which H is the Heaviside step function, taking a value of zero when the argument is negative, and a value of unity otherwise. The standard model closure coefficients are used: $\alpha=13/25$, $\beta=\beta_0 \cdot f_\beta$, $\beta_0 = 0.0708$, $\beta^*=9/100$, $\sigma=1/2$, $\sigma^*=3/5$, $\sigma_{d0}=1/8$ and f_β.

$$f_\beta = \frac{1 + 85\chi_\omega}{1 + 100\chi_\omega}, \qquad \chi_\omega = \left| \frac{\Omega_{ij}\Omega_{jk}S_{ki}}{(\beta^*\omega)^3} \right|, \qquad \Omega_{ij} = \frac{1}{2}\left(\frac{\partial u_i}{\partial x_j} - \frac{\partial u_j}{\partial x_i} \right)$$

(12)

Boundary conditions

At friction wall boundaries, a no-slip condition is imposed whereby velocities are set to zero. Alternatively, Neumann conditions are applied to the three components of the velocity and scalar hydrodynamic quantities at the symmetry boundaries such as top and side boundaries. In the case of waves, the flow is approximated by an oscillatory flow, as will be detailed later. At the outlet (right hand boundary), zero-gradient boundary conditions are imposed for all quantities. At the seabed boundary, the friction velocity U_f is determined from the tangential velocity at the nearest cell center, using the Cebeci and Chang (1978) velocity profile, a generalized version of the van Driest (1956) profile extended to cover all three kinds of boundary categories, smooth, transitional, and rough.

$$\frac{u}{U_f} = 2\int_0^{y_c^+} \frac{dy^+}{1 + \left[1 + 4\kappa^2(y^+ + \Delta y_{cc}^+)^2 C\right]^{1/2}}, \tag{13}$$

$$C = \left[1 - \exp(-(y^+ + \Delta y_{cc}^+)/25)\right]^2 \tag{14}$$

$$\Delta y_{cc}^+ = 0.9\left[\sqrt{k_s^+} - k_s^+ \exp\left(-\frac{k_s^+}{6}\right)\right] \tag{15}$$

in which $y_c^+ = y_c U_f/v$ is the normal distance from the wall to the nearest cell center in wall coordinates ($y_c = \Delta y/2$), with Δy being the cell thickness, $\Delta y^+ = \Delta y \cdot U_f/v$ is the thickness of the near-wall cell in wall coordinates, κ is the von Karman constant (=0.4), $k_s^+ = k_s \cdot U_f/v$ is Nikuradse's equivalent sand roughness in wall coordinates ($k_s = 2.5d$), d being the sediment grain size. Subsequently, the friction velocity obtained in this way is used in the following wall functions for the boundary conditions for k and ω, in the cells nearest to the wall in this case:

$$\frac{k}{U_f^2} = \min\left\{A\Delta y^{+2}, \frac{1}{\sqrt{\beta^*}}\right\}, \tag{16}$$

$$\frac{\omega v}{U_f^2} = \max\left\{\frac{B}{\Delta y^{+2}}, \frac{1}{\sqrt{\beta^*}\kappa\Delta y^+}\right\}. \tag{17}$$

The surface of the structure (pile) is modelled as smooth walls, and the friction velocity at the surface of the structure is determined from the tangential velocity at the nearest cell center based on the profile of Cebeci and Chang (1978), in the same way as described in the preceding paragraph. A similar use of k-ω turbulence closures within flow around and scour beneath pipelines can be found e.g. in Liang and Cheng (2005a and b).

Finally, the boundary condition at the inlet for current flow conditions is obtained from a preliminary hydrodynamic simulation where the flow is driven by a body force for the domain without the presence of the structure. Regarding the wave flow boundary conditions, in order to drive desired oscillatory wave flow conditions, at the left hand boundary the following boundary conditions, taken from Liang and Cheng (2005a), are imposed:

$$u = U_m \sin\left(\frac{2\pi}{T_w}\right), \qquad v = 0 \tag{18}$$

$$k = k_m\left[\sin\left(\frac{2\pi}{T_w}t\right)\right]^2, \qquad k_m = 0.0005U_m^2 \tag{19}$$

$$\omega = \omega_m\left|\sin\left(\frac{2\pi}{T_w}t\right)\right|, \qquad \omega_m = \frac{k_m}{100v} \tag{20}$$

in which U_m is the maximum free stream velocity, and T_w is the wave period. At the opposite right hand boundary, zero-gradient boundary conditions are imposed.

Computational mesh

The computational domain is discretized into finite volumes of quadrilateral blocks in varying shapes and dimensions. Figure 1 shows a detailed picture of the mesh used. During the computations, the mesh is continuously updated to adjust the changes of bed topography.
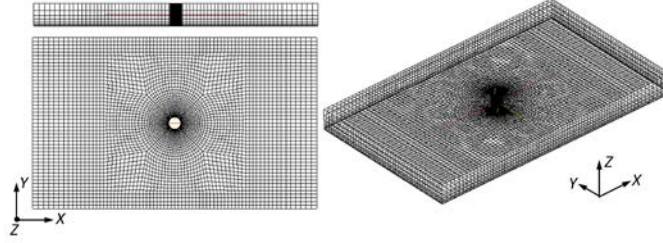

Figure 1. Computational mesh used for the rigid-bed calculations for the pile problem.

The computational domain used in the simulations given here has the following dimensions: Length, $L=20D$, Width, $W=15D$, and Height, $H=2D$ where D is the pile diameter. The total number of cells is $O(10^5)$ in the simulations. As an example for the computational times required, a fully-coupled morphological calculation lasting 1 minute of physical time requires approximately 10 days of CPU time using eight processors.

MORPHOLOGIC MODEL

Sediment transport. Bedload and suspended load

The present study adopts Roulund et al.'s (2005) approach for the bedload description, which is actually an extension of bedload equation of Engelund and Fredsøe (1976) to a two-dimensional vectorial representation.

The suspended load description, on the other hand, is based on a turbulent diffusion equation of the form

$$\frac{\partial c}{\partial t} + (u_j - w_s \delta_{j3}) \frac{\partial c}{\partial x_j} = \frac{\partial}{\partial x_j} \left[(\nu + \nu_T) \frac{\partial c}{\partial x_j} \right] \tag{21}$$

in which c is the suspended sediment concentration, and w_s is the settling velocity of sediment grains. We note that the kinematic viscosity of fluid, ν, is maintained here for numerical reasons, discussed in Jacobsen et al. (2014).

The preceding equation is solved on a truncated version of main computational mesh used for the hydrodynamic computations. In the truncated mesh, the near-bed cells below the reference level b are removed. Therefore, Eq.(21) is only solved starting from the reference level and above. Below this level sediment transport is considered as bed load and therefore not modelled by Eq. (21) (see Jacobsen et al., 2014, e.g. their Fig. 2, for further details). At the top and at the structure boundaries, a zero-flux condition for concentration is utilized, and for the other boundaries Neumann conditions are applied. At the seabed boundary of the truncated mesh, the concentration at the reference level b is calculated by the method of Engelund and Fredsøe (1976) with

$$c_b(\theta) = \frac{0.6}{(1+1/\lambda_b)^3}, \tag{22}$$

$$\lambda_b^2 = \frac{\kappa^2 \alpha_1^2}{0.013 s \theta} \left(\theta - \theta_c - \frac{\pi}{6} \mu_d p_{EF} \right) \tag{23}$$

$$p_{EF} = \left[1 + \left(\frac{\pi \mu_d}{6(\theta - \theta_c)} \right)^4 \right]^{-1/4} \tag{24}$$

in which λ_b is the so-called linear concentration, p_{EF} is the percentage of grains in motion in the surface layer of the bed, α_1 is a constant relating the reference level to the grain size, $b=\alpha_1 d$, the quantity s is the specific gravity of sediment grains, μ_d is the coefficient of dynamic friction, θ is the Shields parameter, and θ_c is the critical value of the Shields parameter corresponding to the initiation of sediment motion at the bed. The Shields parameter is defined by

$$\theta = \frac{U_f^2}{g(s-1)d} \tag{25}$$

in which g is the acceleration due to gravity. In the calculations, θ_c is calculated, taking into account the bed-slope effect (as in Roulund et al., 2005), with a base-line value (i.e., with no bed-slope effect) being 0.05. Throughout the present work, the reference level is taken as $b=\alpha_1 d=3.5d$, which is somewhat larger than the more traditionally used $b \approx 2d$ (e.g. Fredsøe and Deigaard, 1992). Such a large value for the reference level b has been found necessary to promote enough suspended sediment to induce the scour process. This value agrees well with the top mean vertical position reached by single "bedload" particles, $3.0d$–$3.7d$, found by Sumer and Deigaard (1981); see also Abbott and Francis (1977). Same value, $b=3.5d$, is also used by Fuhrman et al. (2014) in the numerical investigation of scour and backfilling beneath submarine pipelines.

Morphologic model

Morphology of the bed elevation h is based on the sediment continuity (Exner) equation

$$\frac{\partial h}{\partial t} = \frac{1}{1-n}\left[-\frac{\partial (q_B)_i}{\partial x_i} + D + E \right], \qquad i = 1, 2 \tag{26}$$

in which $(q_B)_i$ is the i-th component of the bed-load sediment transport vector, n is the porosity of the sediment bed, D is the deposition and E is the erosion, both associated with the suspended load. Further details of the evaluation of deposition and erosion terms in the above given equation is given in Jacobsen et al. (2014) including corrections for the non-sloping beds. It is to be noted that, in the morphology calculations, the time steps are taken exactly the same as in the hydrodynamic calculations, i.e., the morphology model does not make use of morphological rates averaged over a relatively larger time scales. For the latter, and for the other details of the numerical evaluation of the terms in Eq. (26) (particularly the three terms on the right hand side of Eq.(26)), the reader is referred to Jacobsen et al. (2014).

If left un-checked, the morphologic model can lead to local bed slopes in excess of the angle of repose. To avoid this, the sand slide model described in detail by Roulund et al. (2005) is implemented. In the present work, this sand slide model is activated at positions where the local bed angle exceeds the angle of repose $\varphi_s=32.0$, and is de-activated once the local bed angle is reduced to 30.0. Some local filtering of the bed was applied due to stability reasons, as detailed in Baykal et al. (2014 a and b).

The equations comprising the fully-coupled model outlined above are solved numerically using the open-source CFD toolbox OpenFOAM, version 1.6-ext, making use of a finite volume spatial discretization with a collocated variable arrangement, in conjunction with a standard PIMPLE algorithm.

RESULTS

Observations show that, when the correct conditions exist, a previously generated scour hole around a pile may be backfilled; for example, a scour hole generated by a steady current is backfilled when the flow conditions change from steady current to waves, or to combined waves and current, or wave to smaller wave, as mentioned previously.

With the present model, several backfilling scenarios have been simulated in which the initial scour hole is generated by a steady current, and subsequently the scour hole is backfilled with waves. In this study, the early results of these simulations are presented. The example illustrated in Figure 2 is the backfilling of a scour hole around the monopile generated by steady current over an initially flat bed, when the flow climate is changed from steady current to waves, corresponding to a Keulegan-Carpenter number of, $KC=10$,

$$KC = \frac{U_m T_w}{D} \tag{27}$$

in which U_m is the maximum value of the free-stream velocity of the oscillatory flow, T_w is the period of the oscillatory flow, and D is the diameter of the pile.
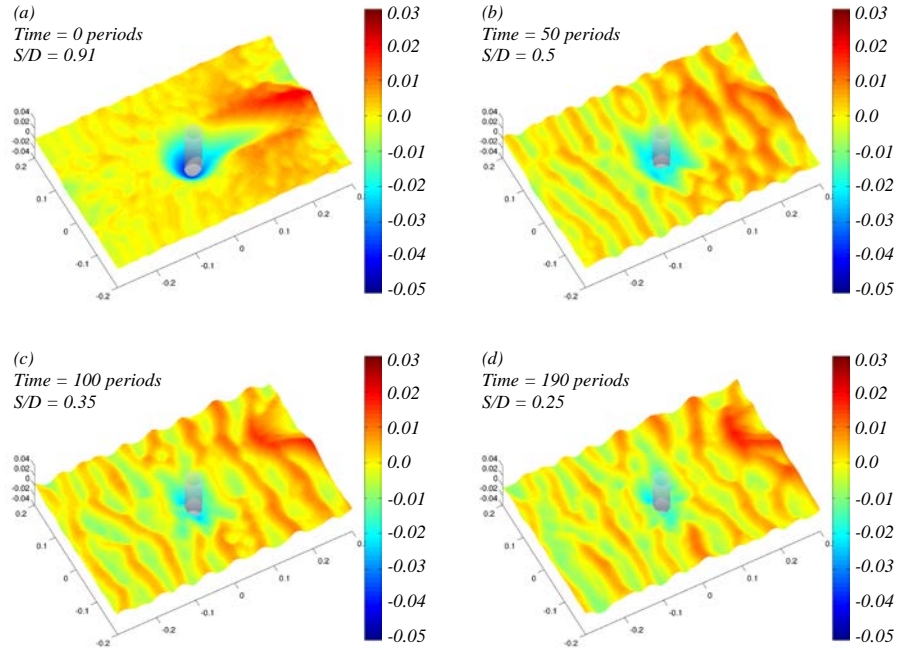

Figure 2. Development of backfilling. Initial scour morphology (Panel Time=0) generated by a current is obtained by the present code. Backfilling occurs with the flow switching from current to waves with *KC*=10.

In the simulations, the median grain size diameter is taken as 0.17 mm and the pile diameter is taken as D=0.04 m. The equilibrium scour profile used as the initial bed profile (Figure 2a, Time=0) for backfilling simulations is achieved with a steady current scour simulation, in which the current velocity is V=41 cm/s, the friction velocity is U_f =1.9 cm/s, and the corresponding Shields parameter is θ=0.13, larger than the critical value for the initiation of motion, θ_c =0.05, implying that the scour is in the live-bed regime. The equilibrium scour depth obtained in the steady current simulation is S/D=0.91 (Figure 2a), where S is the scour depth in front of the pile. This value agrees well with the existing data, for the present water-depth-to-pile-diameter ratio δ/D=2 in the simulation (Sumer and Fredsøe, 2002).

In the backfilling with KC=10, the maximum value of the free-stream velocity of the oscillatory flow in the test is U_m=22.5 cm/s and the wave period is T_w=1.79 s which gives a Keulegan-Carpenter number, KC=10. The Shields parameter is θ=0.15, implying that the live bed conditions prevail, revealed by the presence of ripples in the far field (Figure 2).

Figure 3a shows the time development of backfilling for almost 800 wave periods. The dashed line in Figure 3a represents the equilibrium scour depth for the same test case given in Sumer et al. (2013) in which the equilibrium scour depth of the backfilling process is reported as to be the same as that of the ordinary scour process for the same KC number, revealed by their experiments.

Similar to backfilling simulation with KC=10, the equilibrium scour depth generated by the steady current is also subjected to oscillatory flow with KC=20. In this simulation, the pile and median grain size diameters are the same with the preceding simulation. The maximum value of the free-stream velocity of the oscillatory flow in this test is U_m=20 cm/s, the wave period is T_w=4 s, the Shields parameter is θ=0.09, and the critical value of the Shields parameter is θ_c=0.05. The fact that the Shields parameter is maintained large, larger than the critical value ($\theta > \theta_c$), ensures that the scour hole will be backfilled. Figure 3b displays the time series of the scour depth in front of the pile for the backfilling simulations of KC=10 and KC=20. In Figure 3, the quantity KC_f is the Keulegan-Carpenter number; the sub-indices i and f stand for initial and final, respectively.
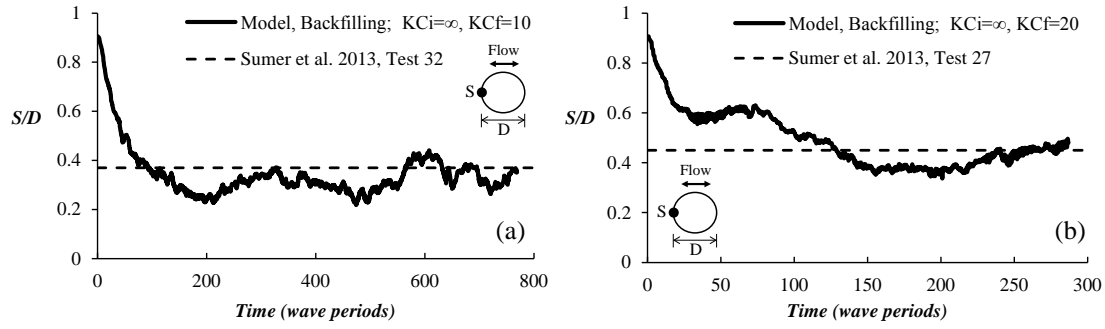
Figure 3. Time series of the scour depth during the backfilling process for the two scenarios with *KC$_f$*=10 (a) and *KC$_f$*=20 (b). Dashed line: Sumer et al.'s (2013) equilibrium scour depth for the given tests.

The time series in Figure 3 indicates that the scour depth experiences a rapid backfilling during the first approximately 30-50 waves, and subsequently the variation of the scour depth flattens out. The rapid, first stage is linked to the backfilling of the scour hole with the sediment coming, for the most part, from the dune that formed at the downstream side of the pile during the current scour before the flow climate is switched to waves. The final stage, on the other hand, presumably corresponds to the stage where the sediment brought into the scour hole is redistributed by the vortex flow.

Figure 4 displays the time scale of the backfilling process corresponding to the simulations described in the preceding paragraphs (Figures 2 and 3). The time scale is defined by (Sumer et al., 2013)

$$S_t = S + (S_i - S)\exp(-\frac{t}{T}) \tag{28}$$

in which T is the time scale of the backfilling process, representing the time period over which a substantial amount of backfilling occurs, defined similar to the time scale of scour processes (Sumer and Fredsøe, 2002). The quantity S_i is the initial scour depth, and S is the equilibrium scour depth corresponding to the backfilling process. The so-called Area Method (Sumer and Fredsøe, 2002; Fuhrman et al., 2014) has been used in the calculation of the time scale. The time scale has been predicted from the times series via integration of the below given

$$T^* = \int_0^{t^*_{\min}} \frac{S - S_{\min}}{S_0 - S_{\min}} dt^* \tag{29}$$

in which $S_{\min}$ is the minimum scour depth, S is the scour depth at any time, S_0 is the scour depth at the beginning of backfilling and the normalized time, t^*, is defined by

$$t^* = \frac{\sqrt{g(s-1)d^3}}{D^2} t \tag{30}$$

in which t is time in seconds, d is median grain size diameter, g is gravitational acceleration and s is specific gravity of sediment.

The solid lines in Figure 4 is reproduced from Eq.16 given in Sumer et al. (2013) and represents the best-fit line for the laboratory data obtained by Sumer et al. (2013). The flow depth to the pile diameter ratio δ/D in the current experiment of Sumer et al. (2013) by which the initial scour hole was generated ($KC_i=\infty$) was around $\delta/D=10$. In this study, this ratio is taken as $\delta/D=2$ for all the simulations to minimize the computational demands. The effect of this ratio, as discussed earlier, is that the scour depth at the end of the scour stage by steady current is less than the one measured by Sumer et al. (2013) where $\delta/D=10$, and therefore the respective time required to fill the scour hole is less too. In Figure 3, θ is the Shields parameter corresponding to the backfilling test.
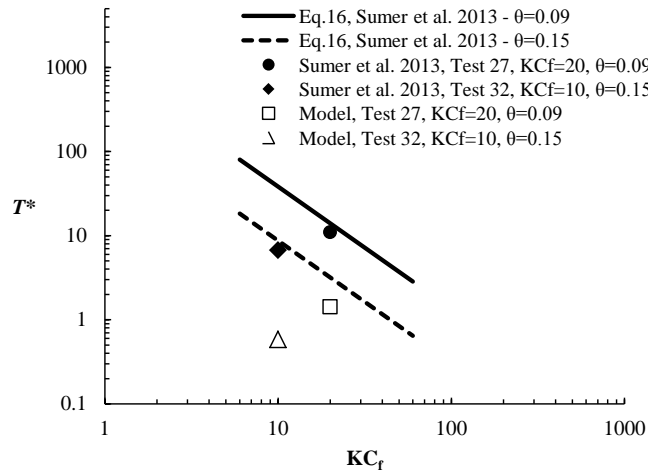
Figure 4. Time scale of the backfilling process for piles with the flow switching from current ($KC_i=\infty$) to waves with θ and KC_f.

Figure 4 shows that the time scale obtained in the present CFD exercise is an order of magnitude smaller than that of Sumer et (2013) al.'s laboratory experiments. The reasons why the present time scale is smaller may be linked to:

(1) The scour tests for currents carried out in Sumer et al. (2013) were conducted for very large times so that the dune at the downstream of the pile was washed away. Therefore, the backfilling in Sumer et (2013) al.'s case took place much more gradually resembling the secondary (slower) part of the time series given in Figure 4. As it is shown in Figure 2a, in case of presence of a dune at the downstream of the pile, the time scale associated with the backfilling stage could be expected to be much smaller compared to the Sumer et (2003) al.'s results.

(2) The water-depth-to-pile-diameter ratio of the present numerical tests is $\delta/D=2$. Sumer and Fredsøe (2002) gives that the scour depth approaches to an asymptotic value for this ratio greater than O(4) (see Fig. 3.26 in Sumer and Fredsøe, 2002). As the initial scour depth obtained in the numerical test is much smaller than the one reported by Sumer et al. (2013), where the δ/D was around O(10), the time scale of backfilling of this scour hole should be again expected to be smaller than the value obtained by Sumer et al. (2013).

(3) In the present numerical tests, the flow in backfilling tests is impulsively started, such that the morphological computations are started after some wave periods while the hydrodynamic and sediment transport computations are carried out. In the physical model experiments, it takes time for the flow to develop, which might be called as the 'ramp time' and is like O($10T_w$), T_w is the wave period. Consequently, having a 'ramp time' would result in a time scale slightly greater than the one without a 'ramp time' as in the case of numerical tests. Furthermore, a numerical simulation for one of the cases given above with a ramp time of $8T_w$ did not result in a significant change in the time scale and resulted in approximately 10% increase in the respective time scale. Moreover, although it is about scour, Dixen et al. (2013) give the results of a numerical test where they increased the flow velocity gradually to its ultimate value rather than starting the flow impulsively. They have shown that the time scale is influenced very significantly in the case of a gradually started flow such that the time scale is increased by a factor of 3-4 compared to an 'impulsively started' flow's (see Dixen et al. 2013, Fig. 22 and Fig. 23c and Table 2).

CONCLUSIONS

A fully-coupled hydrodynamic and morphologic CFD model is presented for simulating scour and backfilling processes around structures. The code has been implemented for two scenarios of backfilling of scour holes around piles.

In the simulations, the initial scour holes are generated numerically by the present code. The scour properties obtained in this way (the scour depth and the scour time scale) are found to be in good agreement with the existing experimental information.

The simulation results show that, regardless of the initial scour hole geometry (flat or scoured), the equilibrium scour depth of the backfilling process will be the same as that of the ordinary scour process for the same Keulegan-Carpenter number, *KC*.

The simulation results also show that the backfilling process occurs in two stages: A rapid first stage, followed by a rather slow backfilling process. The first stage is associated with the backfilling with the sediment originating from the bed feature(s) in the immediate neighbourhood of the initial scour hole.

ACKNOWLEDGEMENTS

REFERENCES

Abbott, J. E. and Francis, J. R. D., (1977). Saltation and suspension trajectories of solid grains in a water stream. Phil. Trans. Roy. Soc. A. 284, 225-254.

Baykal, C., Fuhrman, D. R., Sumer, B. M., Jacobsen, N. G. and Fredsøe, J., (2014a). Numerical investigation of flow and scour around a vertical circular cylinder (To be submitted. Philosophical Transactions of the Royal Society of London A, Special Issue on Advances in Fluid mechanics for Offshore Engineering.)

Baykal, C., Fuhrman, D. R., Sumer, B. M., Jacobsen, N. G. and Fredsøe, J., (2014b). Numerical simulation of flow, scour and backfilling around a vertical circular cylinder in waves and current (To be submitted for journal publication.)

Cebeci, T., and Chang, K. C., (1978). Calculation of incompressible rough-wall boundary-layer flows. AIAA J. 16, 730-735.

Dixen, M., Sumer, B. M. and Fredsøe, J., (2013). Numerical and experimental investigation of flow and scour around a half-buried sphere . Coast Eng. 73, 84-105.

Engelund, F. and Fredsøe, J., (1976). A sediment transport model for straight alluvial channels. Nordic Hydrology 7, 293-306.

Fredsøe, J. and Deigaard, R., (1992). Mechanics of Coastal Sediment Transport. World Scientific Publishing, Singapore.

Fredsøe, J., Sumer, B. M. and Arnskov, M. M., (1992). Time scale for wave/current scour below pipelines. Int. J. Offshore and Polar Eng., 2, 13-17.

Fuhrman, D. R., Baykal, C., Sumer, B. M., Jacobsen, N. G. and Fredsøe, J., (2014). Numerical simulation of wave-induced scour and backfilling processes beneath submarine pipelines. Coastal Eng. 94, 10–22.

Harris, J. M., Whitehouse, R. J. S., and Benson, T. (2010). The time evolution of scour around offshore structures. Maritime Eng., 163(MA1), pp3-17.

Hartvig, P. A., Thomsen, J. M., Frigaard, P., and Andersen, T. L. (2010). Experimental study of the development of scour and backfilling. Coast. Eng. J., 52(2), 157-194.

Jacobsen, N. G., (2011). A full hydro- and morphodynamic description of breaker bar development. Ph.D. thesis, Technical University of Denmark, Kgs. Lyngby.

Jacobsen, N. G., Fredsøe, J. and Jensen, J. H., (2014). Formation and development of a breaker bar under regular waves. Part 1: Model description and hydrodynamics. Coast. Eng. (in press).

Liang, D. and Cheng, L., (2005a). Numerical model for wave-induced scour below a submarine pipeline. J. Waterway, Port, Coastal, Ocean Eng. ASCE, Vol.131, pp193–202.

Liang, D. and Cheng, L., (2005b). Numerical modeling of flow and scour below a pipeline in currents Part I. Flow simulation. Coastal Eng. 52, 25-42.

Nielsen, A. W., and Hansen, E. A. (2007). Time varying wave and current induced scour around offshore wind turbines. Proc., 26th ASME 2007 26th Int. Conf. on Offshore Mechanics and Arctic Engineering, Offshore Mechanics and Arctic Engineering (OMAE), San Diego, pp399-408.

Raaijmakers, T., and Rudolph, D. (2008a). Time-dependent scour development under combined current and wave conditions-Laboratory experiments with online monitoring technique. Proc. 4th Int. Conf. Scour Erosion, ICSE, Tokyo, 152-161.

Raaijmakers, T., and Rudolph, D. (2008b). Time-dependent scour development under combined current and wave conditions-Hindcast of field measurements. Proc. 4th Int. Conf. Scour Erosion, ICSE, Tokyo, pp340-347.

Roulund, A., Sumer, B. M. Fredsøe, J., and Michelsen, J. (2005). Numerical and experimental investigation of flow and scour around a circular pile. Journal of Fluid Mechanics. 534. 351-401.

Sumer, B. M. and Deigaard, R., (1981). Particle motions near the bottom in turbulent flow in an open channel. Part 2. J. Fluid Mech. 109, 311-337.

Sumer, B. M. and Fredsøe, J. (2002). The Mechanics of Scour in the Marine Environment. World Scientific Publishing.

Sumer, B. M., Fredsøe, J. and Christiansen, N. (1992). Scour around a vertical pile in waves. J. Waterway, Port, Coastal, Ocean Eng., ASCE, Vol.117, 15-31.

Sumer, B. M., Christiansen, N. and Fredsøe, J., (1993). Influence of cross section on wave scour around piles. J. Waterway, Port, Coastal and Ocean Eng., ASCE, 119 (5), 477-495.

Sumer, B. M., Petersen, T. U. and Locatelli, L. Fredsøe, J., Musumeci, R. E. and Foti, E. (2013). Backfilling of a scour hole around a pile in waves and current. J. Waterway, Port, Coastal, Ocean Eng., ASCE, Vol.139, pp.9-23.

van Driest, E. R., (1956). On turbulent flow near a wall. J. Aeronautical Sciences 23, 1007-1011, 1036.

Wilcox, D. C., (2006). Turbulence modeling in CFD, 3rd Edition. DCW Industries, Inc., La Canada, California.

Wilcox, D. C., (2008). Formulation of the k-ω turbulence model revisisted. AIAA J. 46, 2823-2838.